JOURNAL OF AIRCRAFT
Vol. 43, No. 2, March–April 2006

Unsteady-Aerodynamic Shape Sensitivities for Airplane Aeroservoelastic Configuration Optimization

P. C. Chen* and D. D. Liu†
ZONA Technology, Scottsdale, Arizona 85251-3540
and
E. Livne‡
University of Washington, Seattle, Washington 98195-2400

Conversion of a general three-dimensional linear unsteady aerodynamic software system to a configuration shape sensitivity code for planar-lifting-surface configurations at subsonic, sonic, supersonic, and hypersonic flows is described. This was achieved by the accomplishment of the following: A global shape design variable sensitivity scheme was formulated based on the complex variable differentiation (CVD) technique. The CVD technique was incorporated into the software system for shape sensitivity analysis. The new capability was validated with the finite difference method and parametric studies on an AGARD swept wing, AGARD wing–tail configuration, a 60-deg swept wing, and an F-5 wing with a control surface. This selection of test cases covers subsonic to hypersonic planar cases in which singularities in the integrals involved are strong, with aerodynamic interference between lifting surfaces, and including supersonic cases with discontinuous pressure distributions. The most challenging aspects of shape sensitivity analysis for linear unsteady aerodynamics have, thus, been addressed.

Introduction

THE step from sizing optimization to shape optimization is crucial at the conceptual and preliminary stages of the design of aerospace vehicles.[1] In sizing optimization of flight vehicles, planform geometry (configuration shape) and topology of the vehicle and its internal structure are fixed. Design variables include cross-sectional dimensions of structural members (structures) and jig-shape bending, twist, and camber distributions on lifting surfaces (aerodynamics). Motions of leading-edge and trailing-edge articulated control surfaces at different maneuver conditions, or equivalent controlled out-of-plane deformations of lifting surfaces due to action of distributed strain-actuators, can also serve as part of the set of sizing-type design variables for all cases in which linearized steady and unsteady aerodynamics around three-dimensional vehicle configurations can be used. In the case of configuration shape optimization, the planform of a flight vehicle is allowed to change in addition to allowed sizing changes in cross-sectional dimensions of structural members, camber distribution (jig shape), and controlled out-of-plane deformations. Thus, span, aspect ratio, sweep, taper ratio, dihedral of trapezoidal wing segments; locations of lifting surfaces on a fuselage or with respect to each other; size and location of control surfaces; or any other geometrical variables defining the shape of wings and control surfaces can all serve as planform shape design variables.

Analytical and computational developments in the area of structural sizing and shape optimization[2,3] have now reached a point where a number of industry-standard commercial finite element based structural optimization codes are already widely used. For example, the GENESIS[4] and MSC/NASTRAN[5] codes offer shape-as well as sizing-type optimization and are examples of this type of technology. In the aerodynamics area, however, this is not the case.

Significant progress has been made over the last 15 years in the area of flight vehicle aerodynamic shape optimization using Euler-based and even Navier–Stokes computational fluid dynamics (CFD) solvers.[6–11] The focus has been the steady aerodynamics of three-dimensional configurations subject to a small number of design constraints, such as constraints on drag, lift, moments, etc. Extension to aerodynamic/structure interaction, with CFD-based aerodynamics and finite element- (FE-)based structural modeling, is still at the early research stage,[10,11] and it is already clear that when used for industry level design and development, this technology would require a massive computational effort.

For flutter and dynamic aeroservoelastic design considerations to be included as an integral part of any design optimization effort of new configurations (that is, when time-dependent flows have to be repeatedly calculated), computational aerodynamic tools based on linearized unsteady aerodynamic modeling still serve as the backbone of any aeroelastic and aeroservoelastic clearance effort. These methods will continue to form the foundation of dynamic-aeroelasticity work for high-speed flight vehicles in the foreseeable future. Both in the steady case (for aeroelastic loads evaluation in a large number of load conditions, using correction techniques, if necessary) and the unsteady case (flutter, aeroservoelastic stability, gust response, dynamic response, ride comfort, handling qualities, etc.), linearized computational steady and unsteady aerodynamics is now at a stage where it can be used effectively not only for the analysis of given configurations, but for the design of evolving ones.

Unfortunately, the development of design-oriented steady and unsteady aerodynamic analysis capability for aeroelastic/aeroservoelastic work lags significantly behind developments in structural design-oriented analysis. The results of only a minimal number of research efforts were reported with focus on obtaining planform shape sensitivities and reduced-order approximations, important elements of design oriented analysis, for general three-dimensional lifting surface configurations.[12–18] For configurations with control surfaces in which the control surfaces might be changing size and location during optimization, the results of only one research effort were reported.[15–17]

Not surprisingly, in practically all multidisciplinary design optimization studies of flight vehicle configurations carried out to date where the overall shape of the vehicle was allowed to change, dynamic aeroelastic or aeroservoelastic constraints were left out. The

Presented as Paper 2004-1759 at the AIAA/ASME/ASCE/ASC/AHS Structures, Structural Dynamics, and Materials Conference, Palm Springs, CA, 19–22 April 2000; received 11 April 2004; revision received 27 January 2005; accepted for publication 31 January 2005.

*Vice President. Member AIAA.
†President. Fellow AIAA.
‡Professor, Department of Aeronautics and Astronautics, Seattle, WA 98195-2400. Associate Fellow AIAA.

same applies to constraints on dynamic stresses due to gusts, control system power requirements for flight in turbulence, ride comfort, and handling qualities, all extremely important in high-speed flight and, especially, in large transonic and supersonic transports.

The goal of the development effort described here is to create a general industry-standard design-oriented steady- and unsteady-aerodynamic analysis capability for the aeroservoelastic aspect of the multidisciplinary shape design optimization of flight vehicles. The term industry-standard is used here to denote model size, reliability, accuracy level, and modeling effectiveness needed for aeroservoelastic clearance of real, complex, three-dimensional configurations to meet industry standards and requirements. The term design-oriented aerodynamic analysis denotes a set of computational aerodynamic tools which has, in addition to its standard analysis capability, also the capability to calculate sensitivities of all aerodynamic pressures, loads, and generalized forces with respect to all user-defined configuration shape design variables. Sensitivity analysis must include, in addition, derivatives with respect to structural changes on a fixed planform (leading to mode shape variations), or sensitivities with respect to aerodynamic parameters, such as Mach number and reduced frequency.

Additional considerations in the creation of the new design-oriented steady- and unsteady-aerodynamic capability are as follows: It has to cover a wide Mach number range, from low subsonic flight to hypersonic flight. Additionally, it has to be modular. That is, it has to be created in a way that will make it easy to interface with commercial and government codes covering the structures and structural dynamics disciplines. The resulting capability will then fit smoothly into any flight vehicle multidisciplinary optimization (MDO) system and will be able to communicate with a variety of available FE codes.

The present paper describes a proof-of-concept development of a three-dimensional design-oriented unsteady-aerodynamic capability focusing on planar lifting surface configurations. The methodology developed is applied to a general industry standard set of unsteady-aerodynamic codes. Because the planar lifting surface case presents some of the strongest singularities in linear unsteady aerodynamics, it is expected the extensions to body shape variations and wing/body interactions will pose no additional major development problem.

Approaches for Computing Aerodynamic Shape Sensitivities

Sensitivity analysis is a fundamental building block of gradient-based optimization. It is also a fundamental tool for assessing robustness of designs to uncertainties and parameter variations, providing the designer with tools to answer "what if" questions.

For an aerodynamic shape-dependent response function R, the sensitivity with respect to a shape design variable (DV) reads

$$\frac{\partial R}{\partial(\mathrm{DV})} = \frac{\partial R}{\partial X_f}\frac{\partial X_f}{\partial X_s}\frac{\partial X_s}{\partial X_g}\frac{\partial X_g}{\partial(\mathrm{DV})} \tag{1}$$

where X_f denotes the aerodynamic field grid, X_s the surface grid, and X_g the geometry description. For CFD-based sensitivity, the field grid sensitivity with respect to the surface grid is rather complex. Here, with panel-method-based sensitivity, this sensitivity becomes simply unity, that is, $\partial X_f/\partial X_s = 1.0$.

For the geometry description X_g of the design configuration, one relies on the methods developed for multidisciplinary shape parameterization.[18] Note that the parameterization techniques can be divided into eight categories: basis vector, domain element, partial differential equation, discrete, polynomial and spline, CAD-based, analytical, and free-form deformation. The suitability criteria are based on the efficiency, effectiveness, ease of implementation, and availability of analytical sensitivities for geometry and grid models.

Many techniques can be adopted to solve Eq. (1) and are listed as follows:

1) Manual differentiation requires intensive derivation and reprogramming.

2) Symbolic differentiation may not be able to remove singularities analytically and may not lead to an efficient code.

3) Automated differentiation (ADIFOR, for example) is a black box approach and may be computationally inefficient.

4) Finite difference method (FDM) has accuracy that is step-size dependent, and the computation time is significant.

5) Semi-analytic technique involves FDM, and therefore, accuracy is step-size dependent.

6) Complex Variable Differentiation (CVD) is a numerically exact method and requires less programming effort.

The CVD technique originated with Lyness and Moler.[19] In the complex variable approach, the variable x of a real function $f(x)$ is replaced by a complex one, $x + ih$. For small h, function $f(x + ih)$ can be expanded into a Taylor's series as follows:

$$f(x+ih) = f(x) + ih\frac{\mathrm{d}f}{\mathrm{d}x} - \frac{h^2}{2}\frac{\mathrm{d}^2 f}{\mathrm{d}x^2} - i\frac{h^3}{6}\frac{\mathrm{d}^3 f}{\mathrm{d}x^3} + \frac{h^4}{24}\frac{\mathrm{d}^4 f}{\mathrm{d}x^4} + \cdots \tag{2}$$

The first and second derivatives of Eq. (2) can be expressed as

$$\frac{\mathrm{d}f}{\mathrm{d}x} = \frac{\mathrm{Im}[f(x+ih)]}{h} + \mathcal{O}(h^2) \tag{3}$$

$$\frac{\mathrm{d}^2 f}{\mathrm{d}x^2} = \frac{2\{f(x) - \mathrm{Re}[f(x+ih)]\}}{h^2} + \mathcal{O}(h^2) \tag{4}$$

where Im and Re denote the imaginary and real parts, respectively. From Eqs. (3) and (4), it can be seen that the derivatives using the complex variable approach only require function evaluations. This feature is very attractive, particularly when the function is sufficiently complicated, in which case to obtain an analytic derivative is cumbersome and error-prone. Unlike the FDM, where the accuracy of the derivative depends on the step size, Eq. (3) shows that the first derivative does not involve differencing two functions followed by magnification of the subtraction error (because of the division by the step size h). Therefore, no roundoff errors exist for the first derivative in the use of the complex variable technique, and the first derivative becomes step-size independent. Note that the second derivative in Eq. (4) is prone to roundoff errors (because of the subtraction of two close numbers), but is not used here. Note that, because CVD does not introduce cancellation (roundoff) error for the first derivative, the step-size h can be as small as machine zero, for instance, $h = 10^{-30}$. Based on Eq. (3), because the truncation error due to Taylor's series is in the order of $h^2 = 10^{-60}$, which becomes a machine zero in a 32-bit computer, CVD does not introduce any numerical approximation and, therefore, can be considered as a numerically exact differentiation technique. To incorporate CVD into an existing code for sensitivities, all variables in the code are declared as complex variables and small imaginary perturbations ($ih \approx i \times 10^{-30}$) in the design parameters are introduced. Division of the imaginary part of the results by h yields the sensitivity.

Based on the preceding discussion, the CVD technique was selected for implementation in the ZAERO software system for the sensitivity computation of unsteady aerodynamics with respect to shape design variables.

Features and Capabilities of a General Three-Dimensional Linear Unsteady Aerodynamic Suite of Computer Tools

The unsteady aerodynamic capability in the ZAERO suite of codes[20–25] is the most general linearized aerodynamic/aeroelastic capability available today especially because of its wings/bodies modeling and a wide Mach number range, from subsonic, sonic, supersonic to hypersonic flight regimes. Realistic air vehicle geometries can be aerodynamically modeled to account for important aeroelastic effects due to blended wing/body, space plane wing/body, missile fins, fixed-wing aircraft with external stores or nacelles, etc. A unified aerodynamic influence coefficient method provides the transonic thickness–shock effect, the sonic solution, the supersonic/hypersonic–thickness effect, etc., in addition to the body/wing interference effect.

Applying CVD to Frequency-Domain Unsteady Aerodynamics

ZAERO unsteady aerodynamics, like most general three-dimensional linear aerodynamics methods, is formulated in the frequency domain, that is, all analyses and computations are complex. To apply CVD, it is required first to convert all complex variable computations to real variable computations. Basically, there are three major tasks necessary when CVD is applied to ZAERO.

The first is manual separation of real and imaginary parts of the aerodynamic influence coefficients A_{ij}. In the subsonic case, the original ZAERO computes the aerodynamic influence coefficients A_{ij} by area integration over "sending" and "receiving" panels[20]

$$A_{ij} = \iint_{\Delta s} e^{ikx_0}\Psi \, \mathrm{d}s \tag{5}$$

where

$$\Psi = \int_{-\infty}^{x_0} \frac{ik(\lambda - MR)}{R}\,\mathrm{d}\lambda$$

Equation (5) can be separated into real and imaginary parts and rewritten as

$$A_{ij} = A_R + iA_I \tag{6}$$

$$A_R = \iint_{\Delta s} \cos(kx_0)\Psi_R - \iint_{\Delta s} \sin(kx_0)\Psi_I \, \mathrm{d}s$$

$$A_I = \iint_{\Delta s} \cos(kx_0)\Psi_I - \iint_{\Delta s} \sin(kx_0)\Psi_R \, \mathrm{d}s \tag{7}$$

where

$$\Psi_R = \int_{-\infty}^{x_0} \frac{\cos k(\lambda - MR)}{R}\,\mathrm{d}\lambda, \qquad \Psi_I = \int_{-\infty}^{x_0} \frac{\sin k(\lambda - MR)}{R}\,\mathrm{d}\lambda \tag{8}$$

Because both A_R and A_I are now real, they are ready for the application of the CVD technique, where all entities will be declared complex for the introduction of the imaginary step size ih. Equations (5–8) are for the subsonic kernel integrals. A similar procedure is applied to the supersonic kernel integrals.

The second task is conversion of complex matrix solver to real matrix solver. The original ZAERO computes the unsteady pressure coefficients C_p by a complex matrix solver,

$$[A_R + iA_I]\{C_{pR} + iC_{pI}\} = \{W_R + iW_I\} \tag{9}$$

where C_p is the unsteady pressure coefficient and W is the normalwash.

To convert the complex matrix solver to a real matrix solver, real and imaginary parts are separated leading to the following equation:

$$\begin{bmatrix} A_R & -A_I \\ A_I & A_R \end{bmatrix} \begin{Bmatrix} C_{pR} \\ C_{pI} \end{Bmatrix} = \begin{Bmatrix} W_R \\ W_I \end{Bmatrix} \tag{10}$$

The third task is declaration of all real variables in the modified ZAERO as complex. By the use of FORTRAN Implicit complex statement, all real variables are converted to complex variables.

Definition of Configuration Shape DVs

The original ZAERO requires eight geometric input parameters to define the planform of a lifting surface. All of these eight parameters are shown in Fig. 1 and can be directly used as configuration shape DVs. This can be achieved by adding a small imaginary part ih, where $h = 10^{-30}$ to those eight parameters one at a time, rendering shape DVs of lifting surfaces to be complex, with small imaginary parts,

$$\mathrm{DV}_k = \mathrm{DV}_{0k} + ih \tag{11a}$$

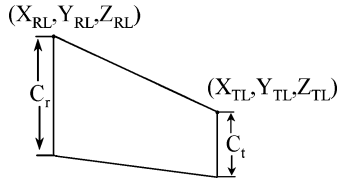

Fig. 1 Eight geometric input parameters to define the planform of a lifting surface.

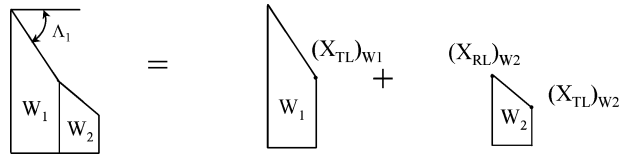

Fig. 2 Shape variable linking for global DV.

where

$$\mathrm{DV}_1 = X_{RL}, \quad \mathrm{DV}_2 = Y_{RL}, \quad \mathrm{DV}_3 = Z_{RL}, \quad \mathrm{DV}_4 = C_r$$
$$\mathrm{DV}_5 = X_{TL}, \quad \mathrm{DV}_6 = Y_{TL}, \quad \mathrm{DV}_7 = Z_{TL}, \quad \mathrm{DV}_8 = C_t \tag{11b}$$

For multiple lifting surface configurations, geometric input parameters of all lifting surfaces can be selectively linked to a set of global DVs. The following example shows that the sensitivity with respect to Λ_1 (Fig. 2) can be obtained by defining $\mathrm{DV} = (X_{TL})_{W1} \bigcup (X_{RL})_{W2} \bigcup (X_{TL})_{W2}$. The $\bigcup$ symbols designate linking of design variables, where a small set of shape DVs determines the shapes of all wing trapezoidal elements. Thus, when sweep angle varies, all coordinates of points on the leading edge vary according to the equations defining their linking to the sweep angle.

Program Architecture for Shape Sensitivities

Figure 3 shows the program architecture for computing the shape sensitivities based on the following equation:

$$\frac{\partial R}{\partial(\mathrm{DV})} = \frac{\partial R}{\partial X_s}\frac{\partial X_s}{\partial X_g}\frac{\partial X_g}{\partial(\mathrm{DV})} \tag{12}$$

Note that because the imaginary perturbation matrix ε is in the order of 10^{-30}, the inverse of the matrix $[A + i\varepsilon]$ can be computed by

$$[A + i\varepsilon]^{-1} = [A]^{-1} - [A]^{-1}[i\varepsilon][A]^{-1} \tag{13}$$

Again, Eq. (13) is numerically exact because the truncation error is in the order of 10^{-60} and is beyond machine zero. Because $[A]^{-1}$ is independent of the shape design variable, it can be computed only once and saved for other shape design variables.

Results and Discussion

Test Cases

Five test cases were selected to validate the new CVD-based lifting surface unsteady aerodynamics configuration shape sensitivities.

The first case tested sensitivities of unsteady pressure coefficients and pressure distributions on an AGARD wing at $M = 1.2$, $k = 0.0$, and $k = 1.0$ (steady and unsteady) and an AGARD wing at $M = 0.8$, $k = 0.0$, and $k = 1.0$ (steady and unsteady).

The second case tested sensitivities of generalized aerodynamic forces on an AGARD wing at $M = 0.8$, $k = 1.0$ with plunge and pitch modes; an AGARD wing at $M = 1.0$, $k = 1.0$ with plunge and pitch modes; an AGARD wing at $M = 1.2$, $k = 1.0$ with plunge and pitch modes; and an AGARD wing at $M = 4.0$, $k = 1.0$ with plunge and pitch modes.

The third test case was for sensitivities of unsteady pressure coefficients of AGARD wing–tail configuration (multiple surfaces, aerodynamic interference).

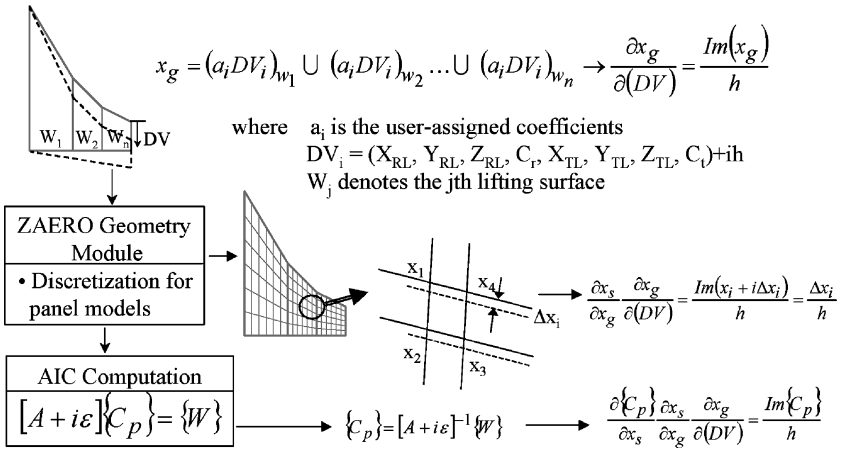

Fig. 3 Program architecture for computing shape sensitivity where subscript *i* is counting index for shape design variables and also used for pure imaginary number.

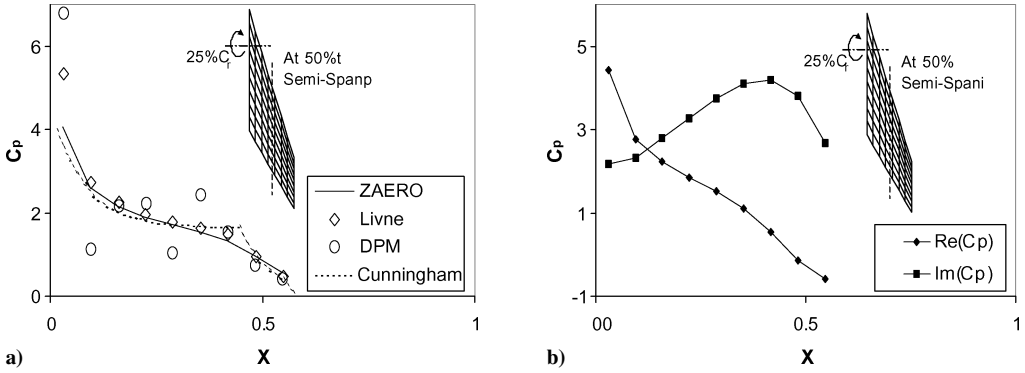

Fig. 4 Unsteady C_p on AGARD wing configuration at $M = 1.2$: a) $k = 0.0$ and b) 1.0.

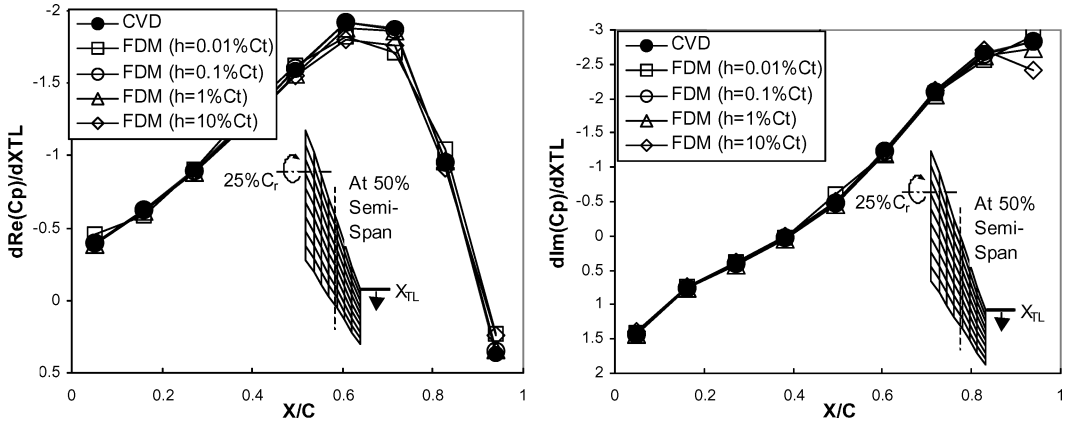

Fig. 5 Sensitivity of unsteady C_p with respect to X_{TL} of AGARD wing at $M = 1.2$ and $k = 1.0$.

The fourth test case was sensitivities of unsteady pressure distributions with known pressure-gradient discontinuities, 60-deg swept wing at $M = \sqrt{2}$.

The fifth test case was of sensitivity of unsteady lift of F-5 wing with control surface with respect to hinge line location at $M = 0.8$, 1.0, and 1.2.

Pressure Distributions for AGARD Wing Configuration at $M = 1.2$ and 0.8 and Reduced Frequencies $k = 0.0$ and $k = 1.0$

Figure 4 shows the unsteady pressure coefficient C_p computed by ZAERO along the 50% semispan of an AGARD wing configuration at $M = 1.2$, $k = 0.0$, and reduced frequency $k = 1.0$ due to a pitch mode about 25% root chord. At $k = 0.0$, ZAERO result agrees very well with those obtained by Li and Livne[16] and Cunningham.[26] The doublet point method (DPM)[27] shows an oscillatory behavior of the unsteady C_p.

The sensitivities of the unsteady C_p on the AGARD wing at $M = 1.2$ and $k = 1.0$ with respect to X_{TL} (Fig. 1) computed by finite differences (FDM) with various step sizes and the CVD ($h = 10^{-30}$) are shown in Fig. 5. Results show that CVD correlates well with FDM when a step size (h) = 0.1% of the tip chord C_t is used for finite differencing. At other step sizes, the results of FDM start deviating from the CVD results, showing, as expected, that the accuracy of FDM is step-size dependent.

Similar comparisons between CVD and FDM for pressure distributions can be seen on Fig. 6, but for the subsonic case ($M = 0.8$ and $k = 1.0$).

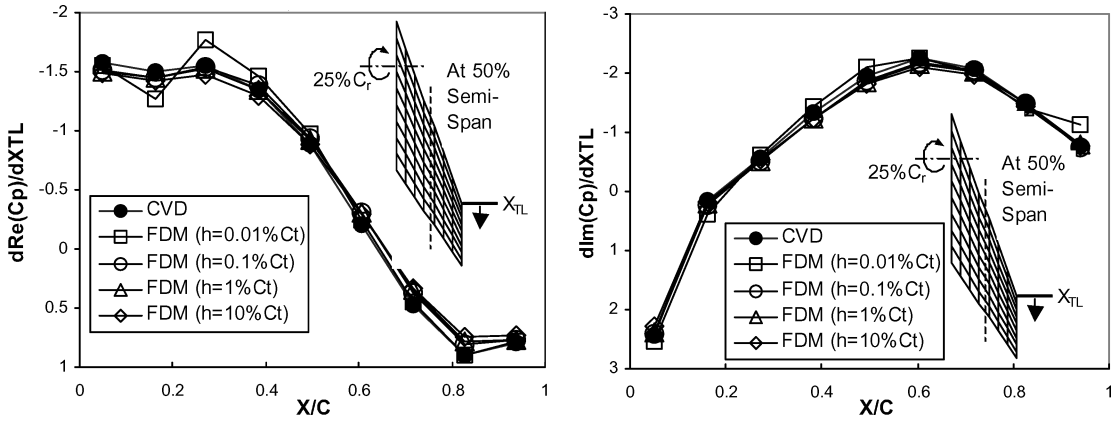

Fig. 6 Sensitivity of unsteady C_p with respect to X_{TL} of AGARD wing at $M = 0.8$ and $k = 1.0$.

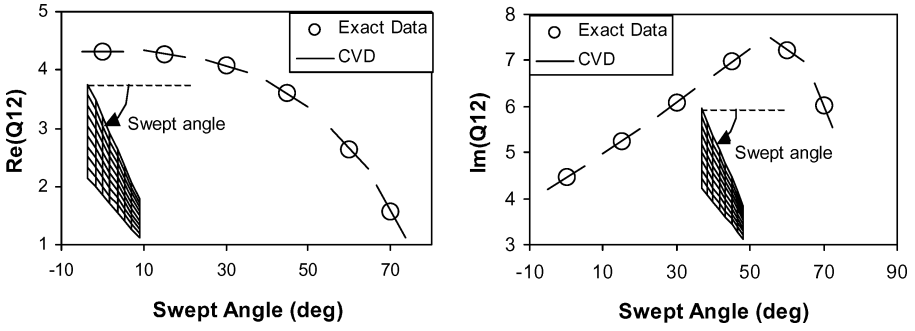

Fig. 7 Sensitivity of unsteady lift AGARD wing at $M = 0.8$ and $k = 1.0$ with respect to sweep angle.

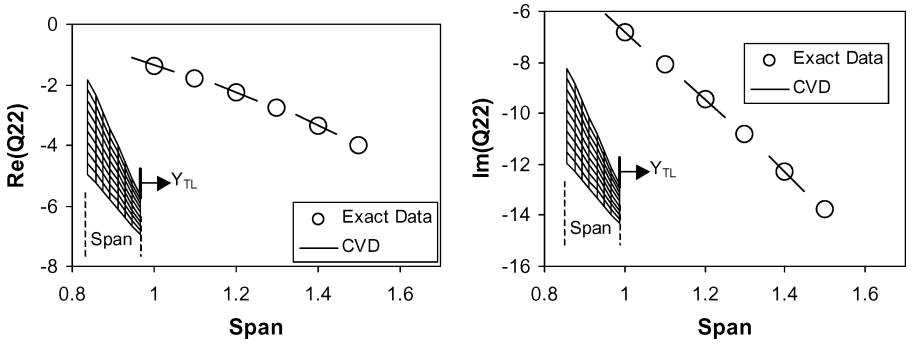

Fig. 8 Sensitivity of unsteady moment AGARD wing at $M = 1.0$ and $k = 1.0$ with respect to span.

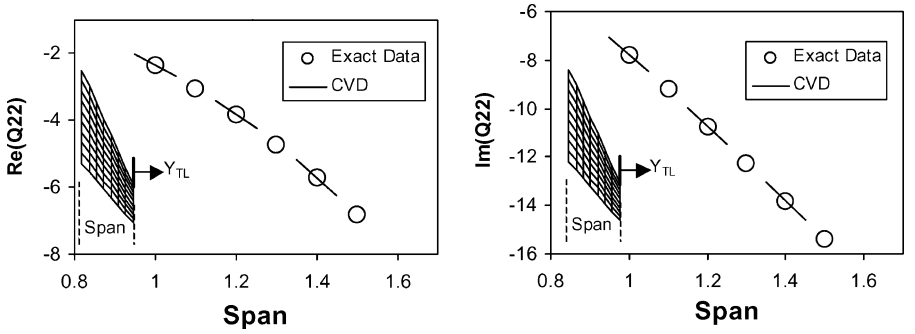

Fig. 9 Sensitivity of unsteady moment AGARD wing at $M = 1.2$ and $k = 1.0$ with respect to span.

Generalized Forces for AGARD Wing Configuration at $M = 0.8$, 1.0, and 1.2 and $k = 1.0$, Rigid-Body Plunge and Pitch Modes

To further verify the CVD sensitivity solutions, parametric studies using full ZAERO analyses (exact data) are used. The generalized forces Q_{12} (lift due to angle of attack) of the AGARD wing at $M = 0.8$ and $k = 1.0$ with plunge and pitch modes are calculated for various sweep angles (open circles in Fig. 7). At these sweep angles, the sensitivities of Q_{12} with respect to the leading-edge sweep angle are computed by CVD and represented by the slope of the solid line segments in Fig. 7. Note that these solid line segments follow the trend of the exact data at various sweep angles very well, verifying the accuracy of CVD for sensitivity of generalized forces.

Similar agreement between CVD and exact data can be seen in Figs. 8 and 9 for the sensitivity of Q_{22} (moment due to rotation) with respect to span at $M = 1.0$ and $k = 1.0$ using the ZSAP method for sonic flows and at $M = 1.2$ and $k = 1.0$ using the ZONA7 method for supersonic flows, respectively.

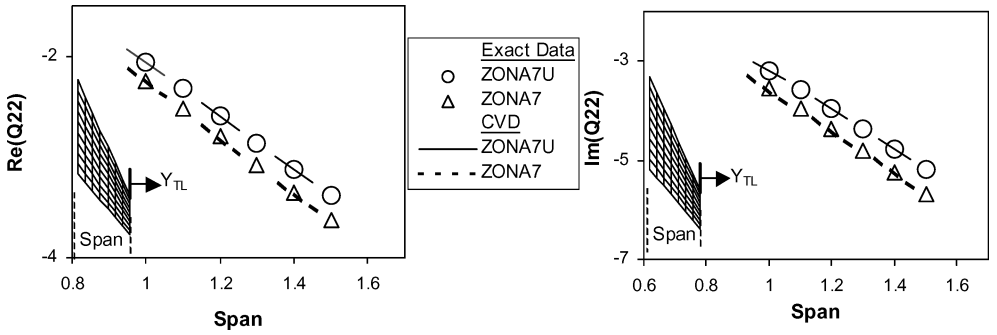

Fig. 10 Sensitivity of unsteady moment AGARD wing with 4% diamond section at $M = 4.0$ and $k = 1.0$ with respect to span.

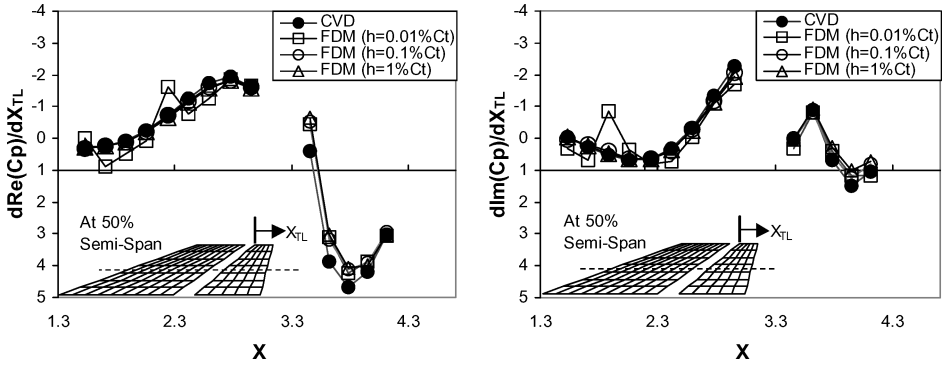

Fig. 11 Sensitivity of unsteady C_p of AGARD wing–tail configuration at $M = 0.8$ and $k = 1.0$ with respect to X_{TL} of tail.

Hypersonic Cases

To validate the CVD technique using the ZONA7U method for hypersonic unsteady flows, a 4% diamond section was added to the AGARD wing to introduce the thickness effects in hypersonic flows. Shown in Fig. 10 is the correlation between the slopes computed by CVD and the exact data using ZONA7U (hypersonic method) for this AGARD wing at $M = 4.0$ and $k = 1.0$ with respect to various spans. In Fig. 10, the results using ZONA7 (linear supersonic method) are also shown. The difference between the ZONA7U and ZONA7 results clearly show the importance of thickness effects in unsteady hypersonic aerodynamics.

Sensitivities of Unsteady Pressure Coefficients of AGARD Wing–Tail Configuration

The objective of this test case was to validate the CVD approach in the multiple-lifting-surface case. Figure 11 shows the sensitivities of unsteady pressure coefficient C_p on an AGARD wing–tail configuration at $M = 0.8$ and $k = 1.0$ with respect to the X_{TL} of the tail (Fig. 1). Good agreement between CVD and FDM (with $h = 1\%$ Ct and 0.1% Ct for the FDM) is obtained. The results of FDM with $h = 0.01\%$ deviate from the CVD results, showing FDM step-size dependency, as expected. The AGARD wing–tail configuration exhibits strong aerodynamic interference between the wing and the closely coupled tail. Success of the new design-oriented planar ZAERO capability in this case demonstrates the power of the new approach in the case of complex configurations involving interfering components.

Sensitivities of Unsteady Pressure Distribution with Known Pressure Gradient Discontinuities

The presence of pressure derivative "jumps" along Mach lines in unsteady supersonic lifting surface flows must be addressed when planform shape variation is considered.[16] In any supersonic panel method, discontinuities in shape sensitivity can be expected when, as a configuration changes shape, aerodynamic boxes move into and out of the Mach cones of other boxes. The objective of the following test case was to demonstrate that the CVD technique could correctly produce nearly numerical singularity in the sensitivity result at discontinuities of the exact data and to show that such pressure derivative discontinuities pose no practical problem. Figure 12a shows the planform of a 60-deg swept wing (Refs. 28 and 29) and the Mach lines and their reflections at $M = \sqrt{2}$. According to the linear supersonic potential theory, the pressure distribution can experience discontinuity or jump when it crosses these Mach waves and reflections. Usually in supersonic flutter analysis, paneling of a configuration is done with uniform meshing, ignoring the lines of pressure singularities. The result is smearing and averaging across the singularity lines, leading to acceptable overall generalized forces, which are integral entities.

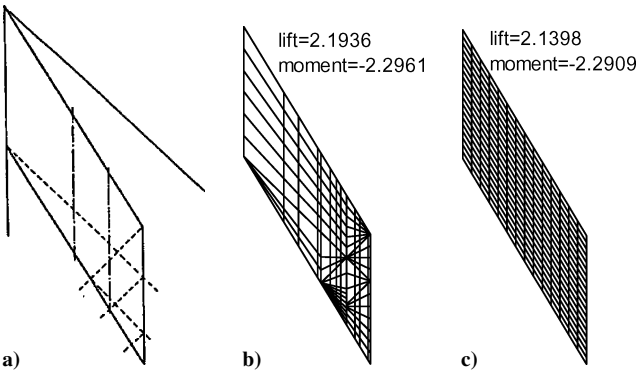

Fig. 12 ZAERO panel models of 60-deg swept wing at $M = \sqrt{2}$: a) Mach waves and their reflections, b) ZAERO Mach wave model, and c) ZAERO regular panel model.

ZAERO, however, can capture these discontinuities and jumps if the panel divisions are defined according to the Mach lines and their reflections. In the case selected for study here, we deliberately meshed the wing in a way that could capture the singularities, and then carried out differentiation with respect to shape using the new planar ZAERO-DO capability. The selected wing was also meshed uniformly, following common practices in supersonic lifting surface unsteady aerodynamics.

Two aerodynamic panel models for the 60-deg swept wing are defined and shown, called Mach-line panel (Fig. 12b) and regular panel (Fig. 12c).

Figure 13 shows C_p due to a unit angle of attack along the 75% semispan of the 60-deg swept wing computed by ZAERO with the Mach-wave panel model and the regular panel model, as well as the exact solution. Note that the correct discontinuities and jumps of C_p are well captured by the Mach-wave panel model, but not by the regular panel model, which smears and averages the distribution, a common feature of all aerodynamic panel methods. The lift and moment computed by the Mach-wave panel are 2.1936 and −2.2961, respectively. The lift and moment by the regular panel are 2.1398 and −2.2909, respectively, which are in very good agreement with those of the Mach-wave panel model. This shows that, for practical applications, the regular panel model is sufficient for providing accurate aerodynamic force and moment coefficients.

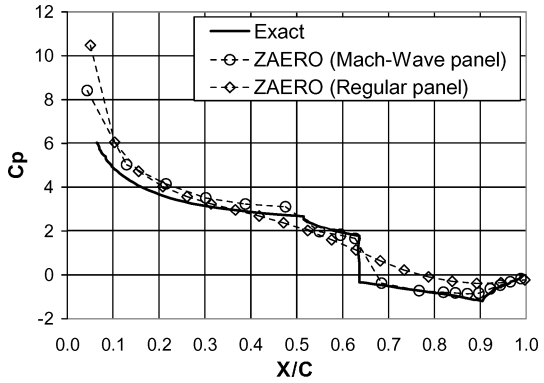

Fig. 13 Discontinuities and jumps in C_p 75% semispan on a 60-deg swept wing at $M = \sqrt{2}$ (Refs. 28 and 29).

Because of the presence of pressure gradient discontinuity along Mach lines, it is expected that the sensitivity of C_p of the 60-deg swept wing at boxes along the Mach lines should be singular. Figure 14 shows the sensitivities of C_p with respect to X_{TL} (Fig. 1) computed by CVD and FDM with various step sizes on the Mach-wave panel model. Indeed, CVD shows spikes at the locations of singularity, which demonstrates the mathematical correctness of the new proof-of-concept ZAERO-DO capability. By contrast, FDM fails to show these spikes.

On the other hand, the sensitivity shown in Fig. 15 of the same case but on the regular panel model is smooth due to the absence of the discontinuity and jumps in C_p gradients. For this case, the FDM results with various step sizes agree well with the CVD results except with $h = 1\%$ Ct.

The sensitivity of lift Q_{12} and moment Q_{22} due to angle of attack of the regular panel model with respect to X_{TL} using CVD and FDM with various step sizes is presented in Fig. 16, which shows the good agreement of the CVD results with the FDM results with $h = 10^{-3}$ and 10^{-2}.

With the use of a uniform mesh (which leads to accurate generalized forces associated with typical structural mode shapes), a parametric study in Figs. 17 and 18 demonstrates the accuracy and reliability of the new method. Shape sensitivities are accurately calculated, as shown by the straight-line segments on Figs. 17 and 18. In Fig. 17, the generalized force is equal to the pitching moment and the exact data refer to solutions obtained by full ZAERO analysis of each configuration. In Fig. 18, generalized force equals lift and the sensitivity of lift on an F-5 wing with respect to hinge line location of the control surface is shown.

Sensitivity of Lift on an F-5 Wing with Respect to Hinge Line Location

The objective of this test case is to demonstrate how to define the hinge line location of a control surface as a shape DV using the design variable linking scheme. Figure 19a shows a F-5 wing

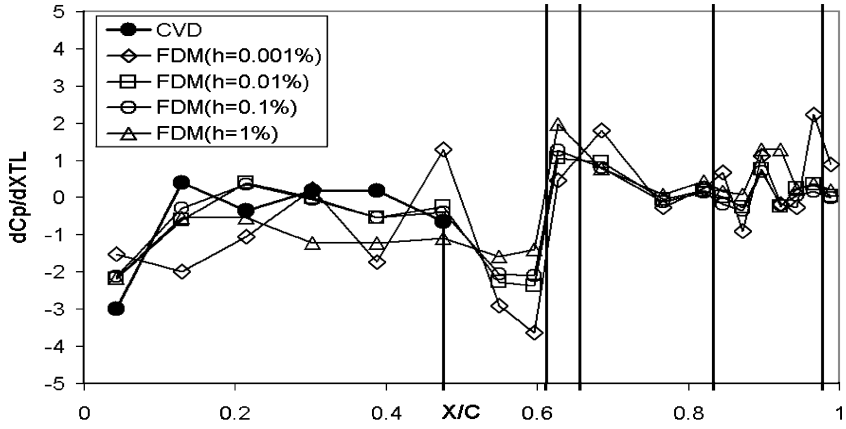

Fig. 14 Sensitivity of C_p 75% semispan on 60-deg swept wing at $M = 1.414$ and $k = 0.0$ on Mach-wave panel model.

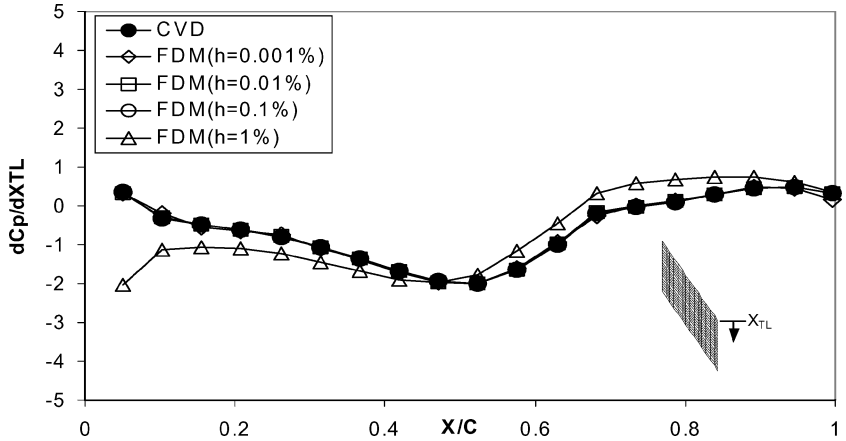

Fig. 15 Sensitivity of C_p at 75% semispan on 60-deg swept wing at $M = 1.414$ and $k = 0.0$ on regular panel model.

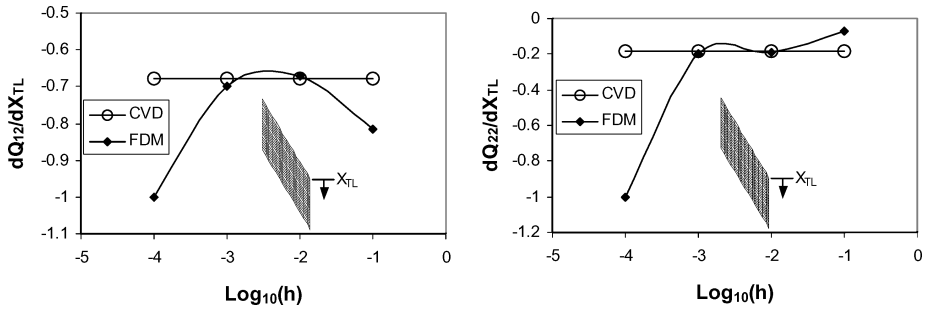

Fig. 16 Sensitivities of lift and moment on 60-deg swept wing at $M = \sqrt{2}$ with respect to X_{TL}: dQ_{22}/dX_{TL} vs step size h.

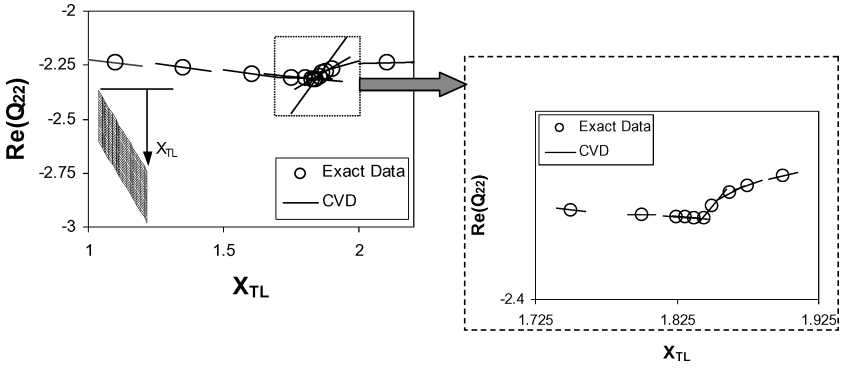

Fig. 17 Validation of new CVD-based shape sensitivities for 60-deg swept wing at $M = 1.414$ (Refs. 28 and 29) using parametric study.

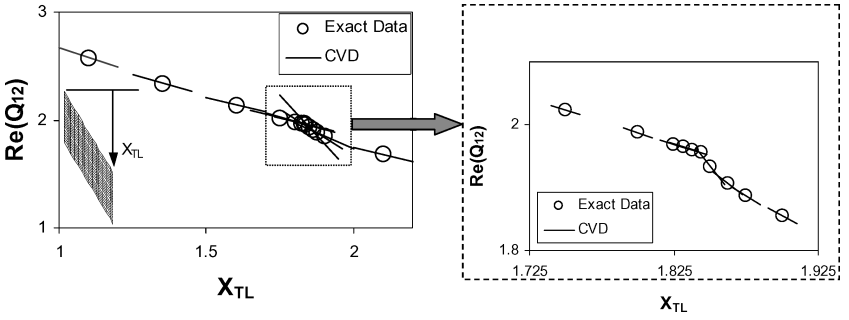

Fig. 18 Validation of new CVD-based shape sensitivities for 60-deg swept wing at $M = 1.414$ using parametric study.

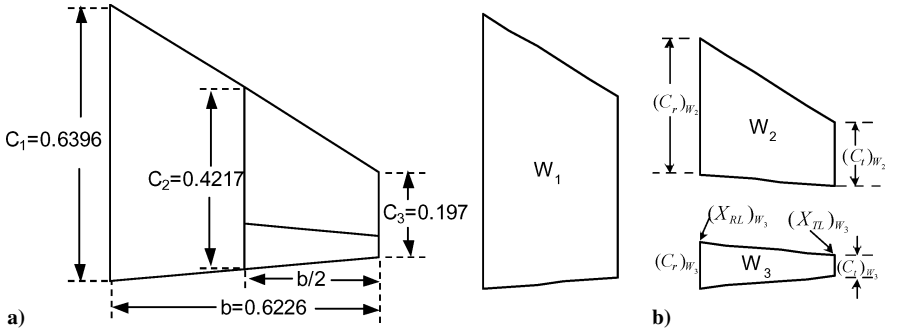

Fig. 19 F-5 wing with trailing-edge control surface: a) planform and b) DVs for variable linking.

with a trailing edge control surface whose hinge line location is along a constant percentage of chord. The constraints of defining the hinge line location as a shape DV variable are that 1) the hinge line location does not alter the chord length, that is, C_2 and C_3 remain unchanged, and 2) the resulting hinge line location must be along a constant percentage of chord.

To define such a shape DV we first model the F-5 wing with three trapezoidal panels as shown in Fig. 19b, denoted as W_1, W_2, and W_3 where the trailing edge of W_2 and leading edge of W_3 coincide to present a hinge line location. In so doing, a global shape DV can be defined as

$$\mathrm{DV} = (C_r)_{W_2} \bigcup (X_{RL})_{W_3} \bigcup - (C_r)_{W_3} \bigcup \left(\frac{C_3}{C_2}\right)(C_T)_{W_2} \times \bigcup \left(\frac{C_3}{C_2}\right)(X_{TL})_{W_3} \bigcup - \left(\frac{C_3}{C_2}\right)(C_t)_{W_3} \tag{14}$$

The $\bigcup$ symbol denotes linking of design variables to a single controlling DV. Here $(C_r)_{W_2} \bigcup (X_{RL})_{W_3} \bigcup - (C_r)_{W_3}$ keeps the total chord length to be C_2, $(C_t)_{W_2} \bigcup (X_{TL})_{W_3} \bigcup - (C_t)_{W_3}$

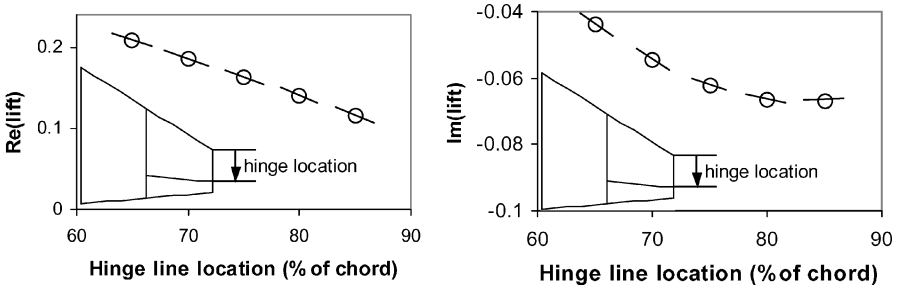

Fig. 20 Sensitivity of unsteady lift of F-5 wing due to flap oscillation at $M = 0.8$ and $k = 1.0$ with respect to hinge line location.

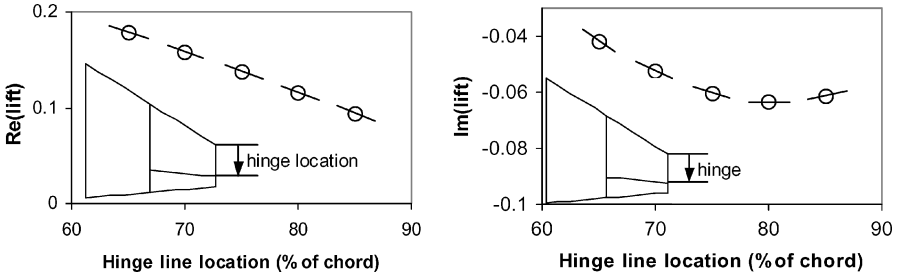

Fig. 21 Sensitivity of unsteady lift of F-5 wing due to flap oscillation at $M = 1.0$ and $k = 1.0$ with respect to hinge line location.

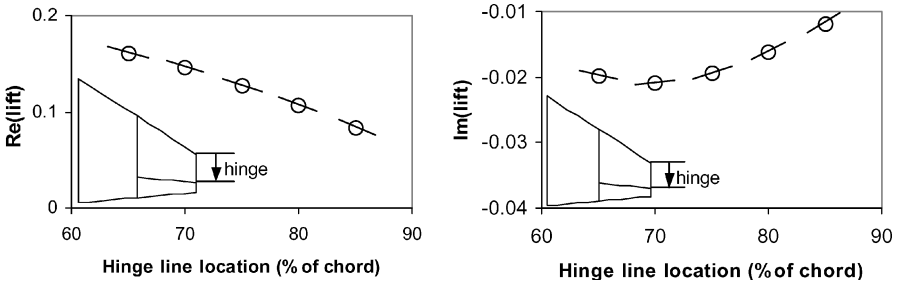

Fig. 22 Sensitivity of unsteady lift of F-5 wing due to flap oscillation at $M = 1.2$ and $k = 1.0$ with respect to hinge line location.

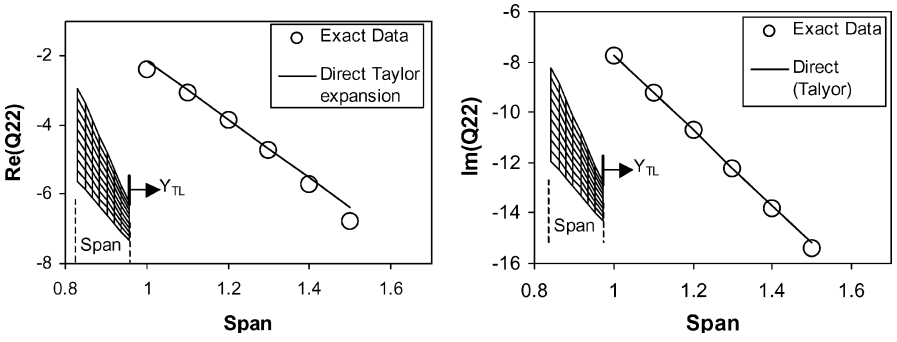

Fig. 23 Comparison between exact data and direct Taylor expansion: AGARD wing configuration at $M = 1.2$ and $k = 1$.

to be C_3, and the ratio C_3/C_2 ensures the hinge line location to be along a constant percentage of chord. The variables $c_{r(W2)}$, $c_{t(W2)}$, $x_{RL(W3)}$, $x_{RT(W3)}$, $c_{r(W3)}$, and $c_{t(W3)}$ are now all linked to a single shape DV and vary with it according to Eq. (14).

The lifts (exact data represented by the open circles) on the entire F-5 wing due to the oscillating trailing edge flap at $k = 1$ and with various hinge line locations are computed by ZONA6 at $M = 0.8$ for subsonic flows (Fig. 20), by ZSAP at $M = 1.0$ for sonic flows (Fig. 21), and by ZONA7 at $M = 1.2$ for supersonic flows (Fig. 22). Also shown in Figs. 20–22 by the slope of the solid line segments are the sensitivities of the lift with respect to the hinge line location computed by CVD. The good correlation between the trend of the solid line segments and exact data clearly demonstrates the accuracy of the CVD technique and the validity of the DV linking scheme.

Taylor Series-Based Approximations

To assess approximation accuracy once sensitivity information becomes available, direct and reciprocal Taylor series approximations were generated and are shown in Figs. 23 and 24. Approximation techniques themselves are well developed, well known, and case dependent.[2,4] When analysis and sensitivity information for a response function is available at a design point 0 with

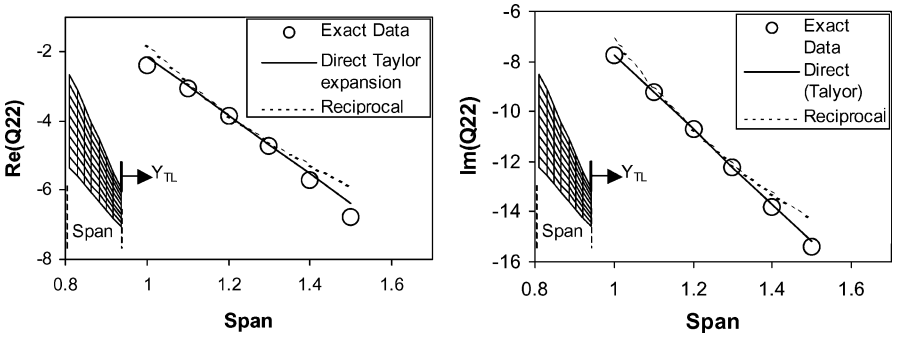

Fig. 24 Comparison among exact data, direct Taylor expansion, and reciprocal formula: AGARD wing configuration at $M = 1.2$ and $k = 1$.

$\{\mathrm{DV}_{1_0}\ \mathrm{DV}_{2_0}\ \ldots\ \mathrm{DV}_{n_0}\}$, a direct Taylor series approximation can be calculated using

$$y \approx y_0 + \sum_{i=1}^{n} \left.\frac{\partial y}{\partial \mathrm{DV}_i}\right|_0 \left(\mathrm{DV}_i - \mathrm{DV}_{i_0}\right) \tag{15}$$

A reciprocal approximation,

$$y \approx y_0 + \sum_{i=1}^{n} \left.\frac{\partial y}{\partial (1/\mathrm{DV}_i)}\right|_0 \left(\frac{1}{\mathrm{DV}_i} - \frac{1}{\mathrm{DV}_{i_0}}\right)$$

$$= y_0 - \sum_{i=1}^{n} \left.\left(\mathrm{DV}_i^2 \frac{\partial y}{\partial \mathrm{DV}_i}\right)\right|_0 \left(\frac{1}{\mathrm{DV}_i} - \frac{1}{\mathrm{DV}_{i_0}}\right) \tag{16}$$

In the test cases analyzed, direct Taylor series approximation performed quite well over a wide range of DV changes, but this, of course, is not a general result.

Conclusions

As part of a proof-of-concept study, a linear panel analysis software system for unsteady aerodynamics of general three-dimensional configurations was successfully converted to a configuration shape sensitivity code in the limited case of planar lifting surface configurations. Subsonic, sonic, supersonic, and hypersonic flows were covered. This was achieved by the accomplishment of the following:

1) A global shape design variable sensitivity scheme was formulated based on the CVD technique.

2) The CVD technique was incorporated into the ZAERO software system for shape sensitivity analysis of planar lifting surfaces.

3) The CVD technique was validated with the FDM and parametric studies on an AGARD swept wing at $M = 0.8$ and 1.2, on an AGARD wing–tail configuration at $M = 0.8$, on a 60-deg swept wing at $M = \sqrt{2}$, and on a F-5 wing with control surface. This selection of test cases covers subsonic, sonic, supersonic, and hypersonic wings, planar cases in which singularities in the integrals involved are strong, aerodynamic interference between lifting surfaces, and supersonic cases with discontinuous pressure distributions. The most challenging aspects of shape sensitivity analysis for linear unsteady aerodynamics have, thus, been addressed.

In future work we hope to extend sensitivity computations from the planar configurations studied here to general nonplanar and wing/body configurations. With the completion of this effort, a new design-oriented unsteady-aerodynamics capability for integrated MDO of air vehicles will become available. Such capability is currently nonexistent, and its absence limits the generality and validity of any design optimization of new air vehicles today.

Acknowledgment

Support by the NASA's Small Business Innovation Research program, Contract NAS1-03028, is gratefully acknowledged.

References

[1]Livne, E., "Integrated Aeroservoelastic Optimization: Status and Progress," *Journal of Aircraft*, Vol. 36, No. 1, 1999, pp. 122–145.

[2]Haftka, R. T., and Gurdal, Z., *Elements of Structural Optimization*, 3rd ed., Martinus Nijhoff, Dordrecht, The Netherlands, 1992.

[3]Vanderplaats, G. N., "Structural Design Optimization Status and Directions," *Journal of Aircraft*, Vol. 36, No. 1, 1999, pp. 11–20.

[4]Vanderplaats, G. N., *Numerical Optimization Techniques for Engineering Design*, Vanderplaats Research and Development, Inc., Colorado Springs, CO; also http://www.vrand.com/genesis_fact.htm.

[5]Scahefferr, H. G., *MSC.Nastran Primer for Linear Analysis*, MSC Software Corp., Santa Ana, CA; also http://www.mscsoftware.com/assets/274_NA_LT-DAT-OPT.pdf.

[6]Jameson, A., "Aerodynamic Design via Control Theory," *Journal of Scientific Computing*, No. 3, 1988, pp. 233–260.

[7]Jameson, A., "Re-Engineering the Design Process Through Computation," *Journal of Aircraft*, Vol. 36, No. 1, 1999, pp. 36–50.

[8]Reuther, J. J., Alonso, A., Jameson, A., Rimlinger, M., and Saunders, D., "Constrained Multipoint Aerodynamic Shape Optimization Using an Adjoint Formulation and Parallel Computers, Part 1," *Journal of Aircraft*, Vol. 36, No. 1, 1999, pp. 51–60.

[9]Reuther, J. J., Alonso, A., Jameson, A., Rimlinger, M., and Saunders, D., "Constrained Multipoint Aerodynamic Shape Optimization Using an Adjoint Formulation and Parallel Computers, Part 2," *Journal of Aircraft*, Vol. 36, No. 1, 1999, pp. 61–74.

[10]Maute, K., Nikbay, M., and Farhat, C., "Coupled Analytical Sensitivity Analysis and Optimization of Three-Dimensional Nonlinear Aeroelastic Systems," *AIAA Journal*, Vol. 39, No. 11, 2001, pp. 2051–2061.

[11]Martins, J. R. R. A., Alonso, J. J., and Reuther, J. J., "High-Fidelity Aero-Structural Design Optimization of a Supersonic Business Jet," AIAA Paper 2002-1483, April 2002.

[12]Yates, C. E., Jr., "Aerodynamic Sensitivities from Subsonic, Sonic, and Supersonic Unsteady, Nonplanar Lifting Surface Theory," NASA TM 100502, Sept. 1987.

[13]Yates, C. E., Jr., "Integral Equation Methods in Steady and Unsteady Subsonic, Transonic and Supersonic Aerodynamics for Interdisciplinary Design," NASA TM 102677, May 1990.

[14]Murthy, D. V., and Kaza, R. V., "Semianalytical Techniques for Sensitivity Analysis of Unsteady Aerodynamic Computations," *Journal of Aircraft*, Vol. 28, No. 8, 1991, pp. 481–488.

[15]Livne, E., and Li, W.-L., "Aeroservoelastic Aspects of Wing/Control Surface Planform Shape Optimization," *AIAA Journal*, Vol. 33, No. 2, 1995, pp. 302–311.

[16]Li, W.-L., and Livne, E., "Analytic Sensitivities and Approximations in Supersonic and Subsonic Wing/Control Surface Unsteady Aerodynamics," *Journal of Aircraft*, Vol. 34, No. 3, 1997, pp. 370–379.

[17]Li, W.-L., and Livne, E., "Design-Oriented Leading-Edge Thrust Force Prediction for Supersonic Lifting Surfaces," *Journal of Aircraft*, Vol. 33, No. 4, 1997, pp. 457–464.

[18]Samareh, J. A., "Survey of Shape Parameterization Techniques for High-Fidelity Multidisciplinary Shape Optimization," *AIAA Journal*, Vol. 39, No. 5, 2001, pp. 877–884.

[19]Lyness, J. N., and Moler, C. B., "Numerical Differentiation of Analytic Functions," *SIAM Journal on Numerical Analysis*, Vol. 4, 1967, pp. 202–210.

[20]Chen, P. C., Lee, H. W., and Liu, D. D., "Unsteady Subsonic Aerodynamics for Bodies and Wings with External Stores Including Wake Effect," *Journal of Aircraft*, Vol. 30, No. 5, 1993, pp. 618–628.

[21]Chen, P. C., and Liu, D. D., "Unsteady Supersonic Computations of Arbitrary Wing–Body Configurations Including External Stores," *Journal of Aircraft*, Vol. 27, No. 2, 1990, pp. 108–116.

[22]Liu, D. D., Chen, P. C., Yao, Z. X., and Sarhaddi, D., "Recent Advances in Lifting Surface Methods," *Royal Aeronautical Journal*, Vol. 100, No. 998, 1996, pp. 327–339.

[23]Chen, P. C., and Liu, D. D., "Unified Hypersonic/Supersonic Panel Method for Aeroelastic Applications to Arbitrary Bodies," *Journal of Aircraft*, Vol. 39, No. 3, 2002, pp. 499–506.

[24]Liu, D. D., Yao, Z. X., Sarhaddi, D., and Chavez, F. R., "From Piston Theory to a Unified Unsteady Hypersonic-Supersonic Lifting Surface Method," *Journal of Aircraft*, Vol. 34, No. 3, 1997.

[25]Chen, P. C., and Liu, D. D., "Unsteady Sonic Aerodynamics Using Acceleration Potential Approach," AIAA Paper 2003-1404, April 2003.

[26]Cunningham, A. M., Jr., "Oscillatory Supersonic Kernel Function Method for Interfering Surfaces," *Journal of Aircraft*, Vol. 11, No. 11, 1974, pp. 664–670.

[27]Ueda, T., and Dowell, E. H., "A New Solution Method for Lifting Surfaces in Subsonic Flow," *AIAA Journal*, Vol. 20, No. 3, 1982, pp. 348–355.

[28]Jones, R. T., and Cohen, D., *High Speed Wing Theory*, Princeton Univ. Press, 1960.

[29]Jones, R. T., *Wing Theory*, Princeton Univ. Press, 1990, p. 103.